Activity statistics in a colloidal glass former: Experimental evidence for a dynamical transition

Bérengère Abou,[1] Rémy Colin,[1] Vivien Lecomte,[2] Estelle Pitard,[3] and Frédéric van Wijland[1,4]
[1]*Laboratoire Matière et Systèmes Complexes, UMR 7057 CNRS-P7, Université Paris Diderot, 10 Rue Alice Domon et Léonie Duquet, 75205 Paris Cedex 13, France*
[2]*LIPhy, Université Grenoble Alpes and CNRS, F-38000 Grenoble, France*
[3]*Laboratoire Charles Coulomb, UMR 5221 CNRS-UM2, Université de Montpellier 2, Place Eugène Bataillon, 34095 Montpellier Cedex 5, France*
[4]*Department of Chemistry, University of California, Berkeley, California 94720, USA*

(Received 28 September 2017; accepted 4 April 2018; published online 25 April 2018)

In a dense colloidal suspension at a volume fraction below the glass transition, we follow the trajectories of an assembly of tracers over a large time window. We define a local activity, which quantifies the local tendency of the system to rearrange. We determine the statistics of the time integrated activity, and we argue that it develops a low activity tail that comes together with the onset of glassy-like behavior and heterogeneous dynamics. These rare events may be interpreted as the reflection of an underlying dynamic phase transition. *Published by AIP Publishing.* https://doi.org/10.1063/1.5006924

I. MOTIVATIONS

In colloidal suspensions, the glass transition refers to the sudden and sharp increase of viscosity as the volume fraction is increased above a typical value. In spite of its accepted name, this phenomenon is not a transition in the standard static sense, according to which a local ordering spontaneously emerges (like between a liquid and a crystal) and for which the properties of the microscopic configurations sampled by the system dramatically change on either side of the transition. Indeed, when looking at the sampled configurations there seems not to be deep structural differences between a glass and the corresponding liquid. In order to characterize and to understand this phenomenon, a number of tools have been proposed. On the theoretical side, these include, but are not limited to, intrinsically dynamical approaches, like the mode-coupling theory or, more recently, a phenomenological picture involving the motion of dynamic facilitation (see the review by Ritort and Sollich[1] or the more recent one by Garrahan, Sollich, and Toninelli, Chap. 10 in Ref. 2). There also exists a purely statics-based proposal, namely, the random first order theory (RFOT) scenario,[3] which depicts the glassy state as originating from a genuinely thermodynamic phenomenon. This theoretical approach is backed by direct equilibrium statistical-mechanical calculations on microscopic systems of interacting particles (either molecular or colloidal), unlike the dynamical facilitation picture which relies only on kinetic rules. Experimental studies aiming at sorting out the appropriate theoretical picture, by testing model assumptions and predictions, are scarce. A remarkable study by Gokhale *et al.*[4,5] does exactly this, by focusing on the nature of local excitations in space and time and by probing point-to-set correlations, showing their consistency with the dynamical facilitation picture. Dynamical facilitation has recently been shown[6–8] to go hand in hand with an unusual signature behavior of the distribution of a number of macroscopic quantities built from the local observables considered in Ref. 4. The twist in defining these macroscopic observables—generically christened *activity*—is to build them by not only summing local spatial quantities over the whole system but above all to integrate the latter over the course of a large time interval so that these exhibit both space and time extensivity. Dealing with the fluctuation properties of space and time extensive observables is the business of the so-called thermodynamic formalism[9] based on spatio-temporal histories. Here, our purpose is neither to go deeper into the mathematical formalism of dynamic facilitation nor to address a direct local quantification of space and time correlations between rearrangement events. Instead we show that these ideas can be practically implemented. It is not only experimentally feasible to measure such a distribution of an extensive observable in a system of interacting colloids but also that telling information can be gathered from such measurements. Concomitantly to the present work, Pinchaipat *et al.*,[10] with polymethylmethacrylate (PMMA) colloidal particles, also found interesting features in the study of time-extensive physical observables.

Our experimental system is a dense suspension of thermosensitive microgels, in which a low density of tracer latex beads has been uniformly dispersed. We track the motion of the tracers in space and time, thus gathering a set of full trajectories $\mathbf{r}_j(t)$ corresponding to each individual tracer j. These are the primary material of our study. These tracers have been shown[11] to be accurate probes for dynamical heterogeneities. The duration $t_{\rm obs}$ of a trajectory is sliced into M lapses of duration Δt, which we choose to be of the order of the time it takes a fluctuation to drive a tracer away by a fraction of its diameter. This is the instanton time introduced in Ref. 7, further discussed in Ref. 12 and concretely used in Ref. 4 to analyze a binary mixture of silica colloids. Following Speck and Chandler[13] we define a tracer-dependent *activity* K as a functional of the trajectories of the observed tracer i

$$K[\mathbf{r}_i](t_{obs}) = \sum_{j=1}^{M=t_{\rm obs}/\Delta t} \Theta\left(||\mathbf{r}_i(j\Delta t) - \mathbf{r}_i((j-1)\Delta t)|| - a\right), \quad (1)$$

where $\Theta(x)$ is the step function and a is a length scale of the order of a fraction of the particle diameter. The purpose of this step function activity K is to count the number of events in which a tracer has been able, in a time Δt, to hop away from its local environment by a distance a. Being the sum of a large number M of local random events (albeit correlated) we expect that the relative fluctuations in K will drop as $\frac{1}{\sqrt{M}}$. But of course M has to be large enough so that K captures the space and time-correlated motion of the tracers. The latter motion will be mediated by the spatially and temporally heterogeneous dynamics. Recent discussions connecting the areas of the system that witness cooperative rearrangement, the structure of facilitated excitations, or soft spots can be found in Ref. 14, for instance. Our purpose in this work is to present the distribution of the activity K as the experiment (where we observe a tracer over time $t_{\rm obs} = M\Delta t$) is repeated a large number of times and over all available tracers. Beyond typical (Gaussian, central-limit related) fluctuations, we aim at quantifying deviations from the Gaussian and to show that these are consistent with the theoretical predictions of Ref. 7. As opposed to earlier studies using a space and time extensive activity, note that ours is extensive in time only. We thus measure directly the complexity of time correlations, which is inherited from space and time correlations of the tracer with its surrounding medium. From a pragmatic point of view, dropping the extensive-in-space nature of the activity helps building much better statistics for atypical events. However, direct comparison with existing theoretical results[7,8] will be slightly less straightforward. The main message to keep in mind is that the distribution of a global, time integrated, physical observable has features that reflect the space-wise and time-wise local peculiarities of the glassy state.

In the following, we describe our experimental system and imaging tool. Then we provide a theoretical section delving into the details of why rare events that tail in the activity distribution is of interest. Our experimental results are then presented and analyzed.

II. MATERIALS AND METHODS

A. Microgel suspension preparation

Our model glass consists of a suspension of thermosensitive microgels, made of the amphiphilic polymer poly(*N*-isopropylacrylamide) (pNIPAm). The suspension, recently investigated in the work of Colin *et al.*,[15] was prepared by mixing small and large microgels with a diameter ratio 1 : 1.8, constant over the investigated temperature range. The bidispersity was used to suppress crystallization. The microgel diameters can be reversibly tuned by varying temperature. When temperature decreases, the particle radius increases and so does the suspension volume fraction. This allows us to explore the various states of the suspension—liquid, supercooled, and glass—with the same sample.[11,16] Within the 20–30 °C range, the pNIPAm particles behave as hydrophilic repulsive soft spheres.

B. Effective volume fraction

The effective volume fraction of our soft microgel suspensions was determined following studies by Richtering and Senff.[17] They showed that pNIPAm microgels, with various degrees of cross-linking and particle size, resemble true hard sphere behavior at low volume fraction, up to effective volume fractions $\Phi < 0.5$ (corresponding to low viscosities up to 10–100 mPa s), and follow a master curve, viscosity versus effective volume fraction. At higher effective volume fractions $\Phi > 0.5$, strong deviations from true hard spheres are observed. Interpenetration of the outer, less cross-linked regions of the soft spheres as well as particle compression occurred. As they discussed in their paper, the deviation from the hard sphere behavior above $\Phi = 0.5$ is not caused by polydispersity effects, but by a soft sphere interaction potential which becomes noticeable when the particles are close to contact.

Here, an effective volume fraction Φ_{30} for the microgel suspension at temperature $T = 30$ °C was determined as follows.[15] We first measured the mean-squared displacement (MSD) of latex probes immersed in the suspension. The MSD was found to increase linearly with time, which defines a diffusion coefficient D, $\Sigma^2(\Delta t) = 4D\Delta t$. A suspension viscosity $\eta = 45$ mPa s was deduced from the Stokes-Einstein relation, $\eta = k_BT/6\pi RD$, expected to be valid at such low viscosity. Using the master curve of Richtering and Senff,[17] an effective volume fraction $\Phi_{30} = 0.49$ was assigned to the microgel suspension at temperature $T = 30$ °C. The volume fractions at lower temperature were then calculated using the relation $\Phi_T = (d(T)/d(T = 30\,^\circ\mathrm{C}))^3\Phi_{30}$, where $d(T)$ is the number-averaged diameter $0.82d_{\rm small} + 0.18d_{\rm large}$ at temperature T. By varying the microgel densities in these suspensions, we obtained a master curve showing that the glass transition onset is reached for effective volume fractions between 0.66 and 0.70 (Appendix A).

C. Supercooled states at $T = 29\,^\circ$C and $T = 27\,^\circ$C

The effective volume fraction was decreased in a quasistatic way, by performing temperature incremental step increases. The suspension was allowed to relax between each step to reach an equilibrium state (as demonstrated by a stationary MSD of the tracers). In our study, we focused on dense suspensions at two temperatures, $T = 29$ °C and $T = 27$ °C, corresponding to two effective volume fractions, $\phi_{29} = 0.54$ (±0.02) and $\phi_{27} = 0.60$ (±0.02). The two effective volume fractions correspond to supercooled states, as demonstrated in Appendix A which describes in more details the behavior of our soft colloid suspensions.

The number-averaged diameters of the particles, defined above, are $\sigma_{29} = 0.887 \pm 0.005$ μm at $T = 29$ °C and $\sigma_{27} = 0.945 \pm 0.010$ μm at $T = 27$ °C. The relative relaxation times, which calculation is detailed in Appendix A, are, respectively, $\tau_{r29} = 128 \pm 7$ and $\tau_{r27} = 649 \pm 32$, obviously between the liquid state [where probability distribution functions (PDFs) of displacement are Gaussian] and the glass state (where there is aging). The $T = 27$ °C is in a deeper supercooled state than the $T = 29$ °C suspension. The suspensions investigated were below the glass transition, as demonstrated by the master curve in Appendix A. Note that we are making use of

relative relaxation times which are useful for making comparisons between the same system at different volume fractions. These times might differ from those one would measure from dynamic light scattering methods.[18]

D. Sample preparation and video recordings

The suspensions were seeded with a low fraction (0.1%) of polystyrene beads (0.994 μm in diameter) which serve as tracers of the dynamics. The suspension is injected into a 3×3 mm^2 chamber made of a microscope slide a coverslip separated by a 250 μm thick adhesive spacer. The chamber was sealed with araldite glue to avoid evaporation and contamination. The samples are observed under bright field transmitted light microscopy at 100X magnification and recorded using a Eosens CMOS camera (field of view 512×512 px^2, 1 px corresponds to 0.138 μm). The temperature of the suspension was maintained constant using a Bioptechs Objective Heater acting on the sample through the immersion oil.

Because of the difference in the diffusion rate when varying volume fraction, images were collected every 0.2 s during 160 s for the $T = 29$ °C suspension (800 images per movie) and every 0.5 s during 500 s at $T = 27$ °C (1000 images per movie). Our value of $t_{\rm obs}$ is fixed to 160 s at $T = 29$ °C or to 500 s at $T = 27$ °C, but we vary M and Δt such that $t_{\rm obs} = M\Delta$ is held fixed. For each volume fraction (temperature $T = 29$ °C and $T = 27$ °C), 10 independent movies were acquired. The fraction of tracers added to the soft particles suspension provides between 50 and 100 tracers in the field of view, depending on the movie. The region of observation was chosen at least 100 μm away from the sample edges to avoid boundary effects.

A self-written analysis software allowed us to track the tracer positions $x(t)$ ans $y(t)$, close to the focus plane, and to calculate all the quantities presented in the following: mean-squared displacement, activity, variance, and skewness. For each probe j in the field of view, the time-averaged quantity was calculated. For each movie, we ensemble-averaged the considered quantity over all the probes present in the field of view. The quantity was finally averaged over the 10 independent movies available for each volume fraction. This allowed us to accumulate a large statistical ensemble for each set of data.

III. DYNAMICAL ACTIVITY

A. Activity of a diffusive ideal gas

As a preliminary investigation, and to set up a reference system, it is instructive to formulate and answer the questions we are interested in for a Brownian particle. We refer the reader to Appendix B for mathematical details. Our purely diffusive Brownian particle has diffusion coefficient D. We ask how the activity of this particle with trajectory $\mathbf{r}(t)$ is distributed in $d = 2$ and $d = 3$ dimensions.

The average activity $\langle K\rangle/M$ of this particle over the time histories reads, in terms of the dimensionless scaling variable $u = \frac{a}{\sqrt{D\Delta t}}$,

$$\frac{\langle K\rangle}{M} = \begin{cases} \mathrm{erfc}\left(\frac{u}{2}\right) + \frac{\mathrm{e}^{-\frac{u^2}{4}}u}{\sqrt{\pi}} & (d=3), \\ \mathrm{e}^{-\frac{u^2}{4}} & (d=2) \end{cases} \tag{2}$$

with the right-hand side in (2) bounded by 0 and 1. We find it of interest to focus on the normalized third cumulant, otherwise known as the skewness κ_3 of the distribution, to quantify the first nontrivial signature of a deviation with respect to the Gaussian distribution,

$$\kappa_3 = \frac{\langle (K - \langle K\rangle)^3\rangle}{[\langle K^2\rangle - \langle K\rangle^2]^{3/2}}. \tag{3}$$

The skewness κ_3, which is a measure of cubic correlations, reads in dimension 3

$$\kappa_3 = \frac{1}{\sqrt{M}} \frac{\mathrm{e}^{-\frac{u^2}{4}}\left(\sqrt{\pi}\mathrm{e}^{\frac{u^2}{4}}\left(2\mathrm{erf}\left(\frac{u}{2}\right)-1\right)-2u\right)}{\sqrt{\sqrt{\pi}\mathrm{e}^{-\frac{u^2}{4}}u\left(2\mathrm{erf}\left(\frac{u}{2}\right)-1\right)-\pi\left(\mathrm{erf}\left(\frac{u}{2}\right)-1\right)\mathrm{erf}\left(\frac{u}{2}\right)-\mathrm{e}^{-\frac{u^2}{2}}u^2}}. \tag{4}$$

A similar calculation carried out in space dimension 2 gives

$$\kappa_3 = \frac{1}{\sqrt{M}} \frac{-2 + \mathrm{e}^{\frac{u^2}{4}}}{\sqrt{-1 + \mathrm{e}^{\frac{u^2}{4}}}}. \tag{5}$$

We will use these expressions for the skewness in Sec. IV as a benchmark to assess the deviation from the diffusive ideal gas behavior.

The idea of examining cubic correlations has emerged recently as a useful tool for the analysis of glassy systems. The work carried out by Crauste-Thibierge *et al.*[19] does exactly that as a function of time [in a similar spirit to studies of the nonlinear susceptibility $\chi_4(t)$]. The observable κ_3 captures instead time-integrated aspects.

B. What are the expected changes in the presence of interactions?

The definition of the activity in our dense suspension with soft repulsive interactions is exactly identical to that appearing in Subsection III A. However the parameters a and Δt entering the activity cannot form a single variable based on the diffusive scaling. The interacting system carries its own space and time scales. In such dense systems, the reference spatial scale is the range of the interaction potential (or the "size" of the particles); however, a hierarchy of relevant time scales show up. The shortest one tells us about local vibrations of the particles around their equilibrium positions. Fast-rattling about a local equilibrium position is not what we are interested in. Instead, the intermediate time scale of interest to us is related to

the time required for a particle to participate in a cooperative rearrangement at the particle scale, leading to another local equilibrium position. Rearrangement events should decrease in frequency and density as the system approaches the glass transition. This is the reason why the macroscopic relaxation rate is seen to increase as temperature is lowered.

While the microscopic mechanism behind the emergence of independent localized excitation patches is unknown, a vast body of theoretical work has been devoted to the study of model systems of excitations with facilitated dynamics.[1] Soft spots are believed to display equilibrium correlations between themselves. However, they exhibit unusually correlated dynamics. One way to capture this property is to investigate the histories of the system configurations over a large time interval. In practice one way to do this is to consider a time extensive quantity and to investigate its fluctuations. The activity is indeed a most relevant measure of the integrated number of excitations over space and time.

In the theoretical literature, the space and time integrated number of excitations up until some observation time $t_{\rm obs}$ is the quantity used[6] in the study of systems with kinetic constraints expressing dynamical facilitation. The activity introduced by Hedges *al.*[7] which we described earlier in Eq. (1) is a proposal adapted to realistic molecular systems. Both in the model lattice systems and in the realistic molecular systems, the probability distribution of the activity displays a double peak structure that is a trademark of supercooled liquids.[20]

In standard equilibrium statistical mechanics, a double peak for the distribution of an order parameter signals a first order transition between two coexisting phases of a system. Given the dynamical nature of the activity, that its distribution displays, a double peak signals the coexistence of two dynamical time evolutions of the system. This corresponds to the "dynamical first order transition" terminology that theoretical works have adopted.

The prediction[6–8] that we wish to investigate here at the experimental level is that the distribution of the activity is a signature of an underlying transition between two dynamical phases: an equilibrium-like phase with homogeneous dynamics and an ergodicity-breaking phase with slow dynamics and low activity. We emphasis that the transition that we study is intrinsically dynamical in the sense that, in contrast to previous experimental work,[21] it does not correspond to an underlying standard phase transition—such transitions being indeed known[22,23] to induce dynamical transitions in a generic manner.

However, the specifics of our experimental analysis differ from the numerical protocol adopted in previous theoretical studies. We have decided to monitor tracers individually and to define a tracer-dependent activity, as is explicit in Eq. (1). At the level of individual tracers, a dynamical first order transition is suggested by the emergence of a secondary peak around the low-activity phase. This can be viewed as a precursor of the real N-body effect that would appear if we monitored collectively the set of tracers. The existence of a low-activity dynamical phase will be manifest in the emergence of a negative excess in the skewness of the activity distribution. Indeed, a negative skewness means a fatter tail for atypically small events.

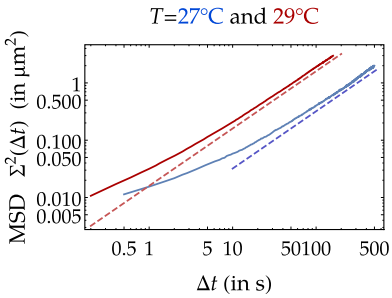

FIG. 1. Mean-squared displacement $\Sigma^2(\Delta t) = \langle(\mathbf{r}_j(t+\Delta t) - \mathbf{r}_j(t))^2\rangle_{t,j}$ of the tracers in the dense microgel suspension at temperatures $T = 27\,^\circ$C (blue) and $T = 29\,^\circ$C (red), as a function of the lag time Δt. For both temperatures, we observe a long-time diffusive behavior (alpha relaxation), preceded by a sub-diffusive behavior at intermediate time scales. At $T = 27\,^\circ$C, the suspension dynamics are much slower than at $T = 29\,^\circ$C. The short-time diffusive behavior is not presented here and can be seen in Ref. 16 and in Appendix A. In the diffusive regime, the MSD slope is 0.017 μm^2/s for the $T = 29\,^\circ$C data and 0.0032 μm^2/s for the $T = 27\,^\circ$C data. The relative relaxation times are, respectively, $\tau_{r29} = 128 \pm 7$ and $\tau_{r27} = 649 \pm 32$ and can be compared to our master curve in Appendix A. Both suspensions are in the supercooled liquid state.

IV. RESULTS

A. Mean-squared displacement and average activity

Figure 1 shows the mean-squared displacement (MSD)

$$\Sigma^2(\Delta t) = \langle(\mathbf{r}_j(t+\Delta t) - \mathbf{r}_j(t))^2\rangle_{t,j} \tag{6}$$

of the tracers as a function of the lag time Δt, in the dense suspension at two temperatures (thus combining the data from both space directions x and y). The average runs over the tracers j and the reference time t. We use Fig. 1 to extract the value Δt_σ such that the mean-squared displacement is equal to the squared diameter of a microgel, $\Sigma^2(\Delta t_\sigma) = \sigma^2$. This value Δt_σ is used in the following for the computation of the probability distribution function (PDF) of the displacement.

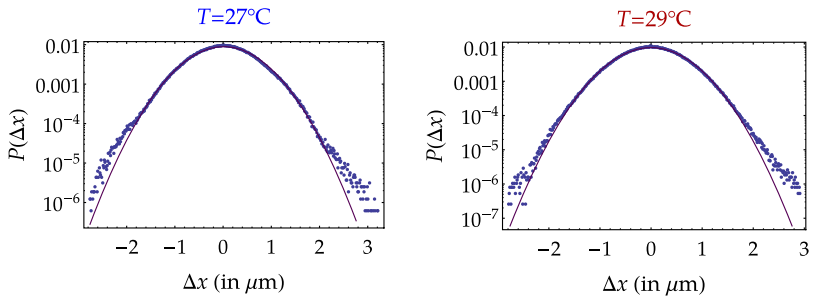

FIG. 2. Probability distribution function of the displacement Δx of the tracers in the dense microgel suspension during Δt_σ, at temperatures $T = 27\,^\circ$C (left) and $T = 29\,^\circ$C (right). For each temperature, the time lapse Δt_σ is fixed by imposing $\Sigma(\Delta t_\sigma) = \frac{1}{2}\sigma$, with σ the microgel diameter. One finds $\Delta t_\sigma \simeq 53$ s and $\Delta t_\sigma \simeq 9.4$ s for $T = 27\,^\circ$C and $T = 29\,^\circ$C, respectively. The PDFs departs from a Gaussian distribution for both temperatures, as extensively discussed in Ref. 11. The solid line represents the Gaussian distribution.

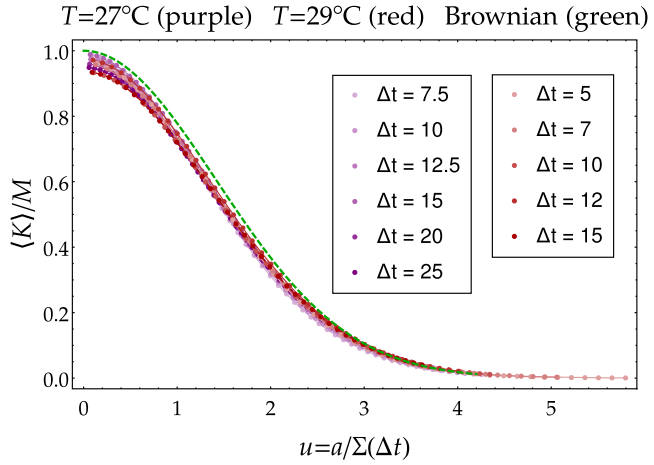

FIG. 3. Average activity $\langle K\rangle/M$ as a function of $u = a/\Sigma(\Delta t)$ at temperatures $T = 29$ °C (red) and $T = 27$ °C (purple). The dashed green curve stands for the Brownian counterpart (2) in dimension $d = 2$. For each temperature/color, the various curves correspond to different choices of Δt. At $T = 27$ °C, the Δt's are such that $\Sigma(\Delta t)/\sigma$ lies between 0.09 and 0.16 and between 0.17 and 0.29 at $T = 29$ °C.

The PDFs of the displacement shown in Fig. 2 deviate from a Gaussian distribution for each temperature studied. This non-Gaussian behavior of the PDF was extensively discussed in Ref. 11 in terms of local heterogeneities of the diffusion coefficient and was shown to be the signature of a supercooled regime. Deviations from the Gaussian emerge after Δx exceeds a threshold value a of the order of 2σ, which corresponds to atypical events. Here, by contrast, we wish to characterize the emergence of dynamical heterogeneities, at scales smaller that 2σ and for non-static observables (intermediate scales).

The average activity $\langle K\rangle/M$ of the tracers immersed in the dense suspension at two temperatures is shown in Fig. 3 as a function of $u = a/\Sigma(\Delta t)$, for different values of Δt. In our data set, M lies between 20 and 66 at $T = 27$ °C and between 11 and 20 at $T = 29$ °C. The average is computed over all the tracers present in the sample, as it is the most direct way experimentally to calculate averages over time histories. One remarks that the experimental results are close to the average activity of a purely diffusive Brownian particle, given by (2), in dimension $d = 2$.[24] One infers from Fig. 3 that the average activity is a poor observable to discriminate between dynamical regimes: Although they exhibit different dynamics (probed by the PDFs, for example), both temperature suspensions and the purely diffusive Brownian particle display a similar activity. Hence, in Sec. IV B, we will search for a macroscopic evidence of dynamical heterogeneities by looking at the full distribution of the activity.

B. Histograms of the activity

In Figs. 4 and 5, we show the histograms of $K/\langle K\rangle$ at both temperatures for varying values of u—smaller than, of the order of, and larger than 1. For $u \sim 1$ [$a \sim \Sigma(\Delta t)$, i.e., for the most probable value of the displacement at fixed Δt], the distribution of activity is found to be symmetric, while it exhibits a pronounced asymmetry when a departs from $\Sigma(\Delta t)$ ($u < 1$ and $u > 1$). Besides, at fixed time lapse Δt, the activity K probes the distribution of jumps larger than a. As a consequence, if $a \lesssim \Sigma(\Delta t)$, one expects K to be larger than if $a \gtrsim \Sigma(\Delta t)$: this is indeed what we observe in Fig. 3.

In a system with dynamical heterogeneities where slow and fast trajectories coexist, the distribution of a space and time extensive activity will exhibit two peaks, of small and large activity. For our observable K, the signature of dynamical heterogeneities is manifested as an asymmetric $P(K)$ biased towards small K. As the system becomes more and more glassy, the width of $P(K)$, as well as the asymmetry of $P(K)$, is expected to increase. In the two following paragraphs, we will then focus on the variance and the skewness of the activity with varying u to investigate such a behavior and detect the emergence of slow trajectories (low activity) for $u > 1$.

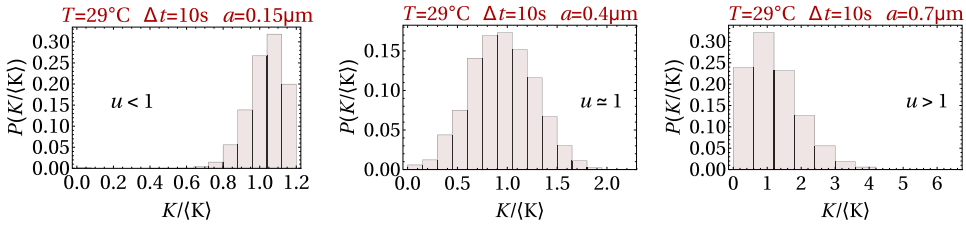

FIG. 4. From left to right: Histogram of the activity at $T = 29$ °C normalized by its average for $a = 0.084\sigma$, $a = 0.22\sigma$, and $a = 0.39\sigma$, respectively. The corresponding values of u are then, respectively, 0.32, 0.87, and 1.52 and those of $\langle K\rangle/M$ are 0.85, 0.43, and 0.095. The time lapse Δt is 10 s. The more symmetric histogram (center) is at value of a of the same order as $\Sigma(\Delta t)$.

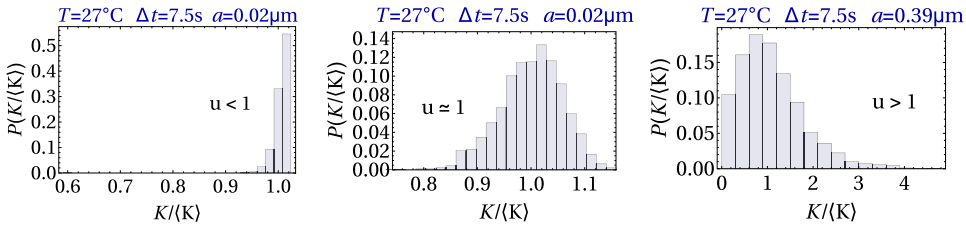

FIG. 5. From left to right: Histogram of the activity at $T = 27$ °C normalized by its average for $a = 0.021\sigma$, $a = 0.085\sigma$, and $a = 0.41\sigma$, respectively. The corresponding values of u are then, respectively, 0.37, 1.50, and 7.35 and those of $\langle K\rangle/M$ are 0.492, 0.361, and 0.0705. The time lapse Δt is 7.5 s. The most symmetric histogram (center) is at the value of a of the same order as $\Sigma(\Delta t)$.

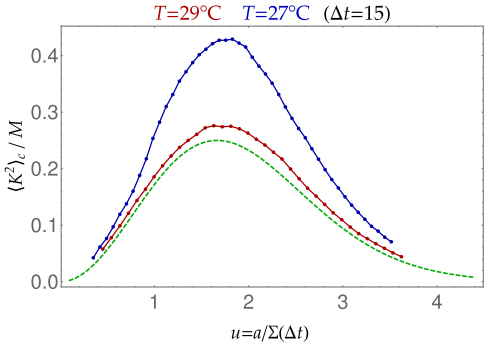

FIG. 6. Mean variance $\langle K^2\rangle_c/M$ as a function of $u = a/\Sigma(\Delta t)$ at temperatures $T = 29$ °C (red) and $T = 27$ °C (blue) for the same time lapse $\Delta t = 15$ s. The dashed green curve stands for the Brownian motion counterpart Eq. (B4) (in dimension $d = 2$).

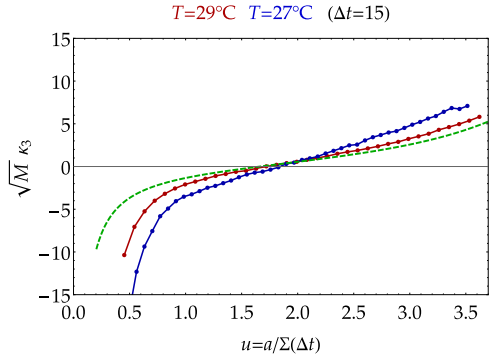

FIG. 8. Scaled skewness $\sqrt{M}\kappa_3$ as a function of $u = a/\Sigma(\Delta t)$ at temperatures $T = 29$ °C (red) and $T = 27$ °C (purple) for the same time lapse $\Delta t = 15$ s. The dashed green curve stands for the Brownian motion counterpart Eq. (5) in dimension $d = 2$.

Unlike what occurs at $T = 29$ °C, asymmetry is slightly more marked at $a \neq \Sigma(\Delta t)$ and this is what we will quantify in Subsection IV C. This is visible with the naked eye only at $u < 1$.

C. Variance of the activity

We compare in Fig. 6 the rescaled variances $\langle K^2\rangle_c/M$ of $P(K)$ in the dense suspension at temperatures $T = 27$ °C and $T = 29$ °C and the variance in the Brownian case [Eq. (B4)], for the same value of the time lapse $\Delta t = 15$ s. In Fig. 7, the variances at each temperature are also plotted for different values of the time lapse Δt. Although the experimental data cannot be directly compared for the same Δt (except for $\Delta t = 15$ s), the variance in the suspension at low temperature $T = 27$ °C is found to be larger than at high temperature $T = 29$ °C (closer to the Brownian one). These results show that the variance increases in a significant way when approaching the glassy regime, indicating $P(K)$ displays a significant broadening, consistent with the increase of dynamical heterogeneities.

We now want to find out whether the corresponding broadening of $P(K)$ is due to a symmetric enlargement of the central peak or whether it is due to the emergence of rare events (on either side of the average).

D. Skewness of the activity

We now investigate the asymmetry of the histograms $P(K)$ by focusing on their skewness. Figure 8 compares the skewness for both temperatures, and for the two-dimensional Brownian case [Eq. (5)], for the same value $\Delta t = 15$ s. Around $u^* \simeq 2$, the skewness is zero for all the curves displayed, in agreement with the symmetric distributions observed in Figs. 4 and 5 for the same value u^*. For lower values $u < u^*$ and larger values $u > u^*$, the skewness departs from zero indicating that the distributions—including the Brownian case—become asymmetric. In particular, in the large u regime ($u > u^*$) where slow trajectories are probed, the asymmetry is found to be significantly larger with decreasing temperature. The wording "slow" refers to those trajectories with rare but large hops. A positive skewness at large u means that in this regime there is an excess of events at above average values of the activity, with respect to a Brownian reference, when $\langle K\rangle$ is small. If we would compare two trajectories, a purely Brownian one and one of a tracer feeling the supercooled regime, sharing the same small value of $\langle K\rangle$, then our analysis shows that the tracer displays more heterogeneous jumps than the benchmark Brownian particle, with more large hops and less small hops. Conversely, $u < u^*$ is in correspondence with large $\langle K\rangle$ and we are thus focusing on smaller sized jumps (which we associate to faster motion). Then the skewness is negative, expressing a distribution of K fatter on the $K < \langle K\rangle$ side, with an excess of smaller sized motion with respect to a Brownian particle when $\langle K\rangle$ is large. And if we again compare a benchmark Brownian particle to our tracer with the same large $\langle K\rangle$ in common, then the tracer exhibits more heterogeneous motion with more cage-like, localized or small amplitude motion than a Brownian particle. Both the $u < u^*$ and $u > u^*$ regimes are consistent with the expected physics, and that of increased heterogeneity as the tracer dynamics departs from a Brownian one.

The excess skewness is the manifestation of an asymmetry in the distribution of activity that originates from a growing number of regions with lower activity (or "inactive domains").

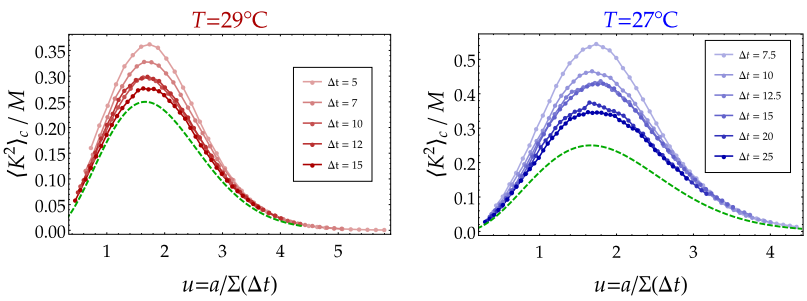

FIG. 7. Mean variance $\langle K^2\rangle_c/M$ as a function of $u = a/\Sigma(\Delta t)$ at temperature $T = 29$ °C (left) and temperature $T = 27$ °C (right). The dashed green curves stand for the Brownian motion counterpart, Eq. (B4) (in dimension $d = 2$). The various curves correspond to different choices of Δt as given in the legend (values in seconds).

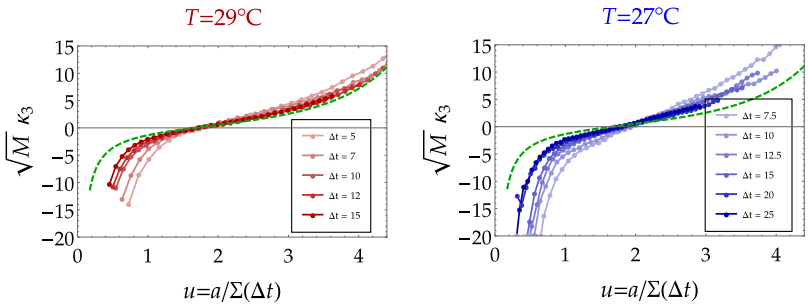

FIG. 9. Scaled skewness $\kappa_3\sqrt{M}$ as a function of $u = a/\Sigma(\Delta t)$ at temperature $T = 29$ °C (left) and temperature $T = 27$ °C (right). The dashed green curves stands for the Brownian motion counterpart Eq. (5). The various curves correspond to different choices of Δt (in s).

Since the extent of such inactive domains is quantified by the skewness amplitude, our results provide a clear experimental evidence of the presence of a larger number of inactive domains present in the suspension when approaching the glassy regime. This effect can also been seen in Fig. 9 where the scaled skewness is plotted for various values of Δt, for both temperatures.

V. DISCUSSION

We have put forward the experimental utility of a dynamical observable, the activity K, in order to quantify the approach to the glassy regime in dense microgel suspensions. In the most heterogeneous phase, the distribution $P(K)$ of activity displays a secondary structure at small values of K. This is a signature of long-lived slower than average regions in the system. Our main result is that, even far from the glass, in the supercooled regime, one observes the existence of heterogeneities in the statistics of K, all the more so as one approaches the glass transition.

We have compared the experimental results for $P(K)$ to the analytical results for a model of independent Brownian diffusers. The average of K (which is fully determined by the static properties of the system), as expected, does not allow us to distinguish the experimental tracers from the Brownian diffusers. The mean variance of K does display a difference: it increases as we go deeper in the glassy phase (by decreasing the temperature), but it does not allow us to distinguish between an effective broadening of the distribution of K and the emergence of a dynamical phase with lower values of the activity. With the single-tracer observable K that we use, it is unlikely that a true dynamical phase transition occurs anyhow. It should instead resemble[25,26] a crossover with a smooth emergence of an excess of inactive events, and this is what we see.

The skewness of K proves to be the most relevant statistical observable, when measured as a function of the scaling variable $u = a/\Sigma(t)$. Using the diffusive ideal gas as a reference allows us to endow the deviations from the diffusive ideal gas with the meaning of effective number of *independent* degrees of freedom. In other words, since the form of the skewness are comparable in our system and in the ideal gas (see Figs. 8 and 9), we can interpret the measure of the skewness in our interacting system as that of an ideal gas that presents a different number of particles, that counts the effective independent degrees of freedom of the system. At $T = 29$ °C (the liquid-like sample), we see that this number does not notably vary with the choice of Δt, for the whole $u > u^*$ range. By contrast, at $T = 27$ °C (deeper in the supercooled liquid state hence more heterogeneous), we do see a greater sensitivity with respect to Δt over the while u range. Such increased sensitivity of the skewness is similar to the increase of the susceptibility at the approach of a critical point of a thermodynamic transition. Keeping in mind that the skewness we consider is a dynamical observable, this clearly illustrates in our system the approach of a dynamical transition as the temperature is lowered.

The distribution of activity for Brownian particles is obviously asymmetric (because it probes atypical events which have no reason to be Gaussian). A positive skewness indicates an excess of larger-than-average events. For $u > u^*$, not only do we have a positive skewness but above all the latter is in large excess over the Brownian curve. In the glassy state, there is an excess of longer range directed events.

Our interest goes now to the skewness falling below the Brownian level at values of $u < u^*$. In this u regime (u a fraction of unity), we know that a really has the meaning of a cage size. And we see that there is a sharp increase in less-than-average active events. This observation is consistent with the emergence of a secondary low activity peak in the activity distribution, without having to characterize the large deviations of $P(K)$ (which are difficult to measure in experiments). What we witness here is the build-up of inactive events that leads to fatter-than-Brownian tails in inactive events.

In Appendix C, we show that our results are robust and fully consistent with what can be inferred from experimental data by Weeks *et al.*[27] This comparison illustrates the robustness of our proposed analysis, which still holds although the data of Ref. 27 present the following differences: (i) the tracking is performed in dimension $d = 3$ instead of our effective $d = 2$, (ii) instead of specific tracers, all particles of the system are tracked, and (iii) the acquisition is made on shorter trajectories in time, but with larger statistics.

ACKNOWLEDGMENTS

We warmly thank Eric Weeks for allowing us to make use of his data and for his comments on an earlier version of this manuscript. V.L. acknowledges support by the ERC Starting Grant No. 680275 MALIG and by the No. ANR-15-CE40-0020-03 Grant LSD.

APPENDIX A: MICROGEL SUSPENSION BEHAVIOR WITH VOLUME FRACTION

Our purpose here is to describe the behavior of our microgel suspensions for various effective volume fractions Φ_{eff} or reciprocally relative relaxation times τ_r (dimensionless).

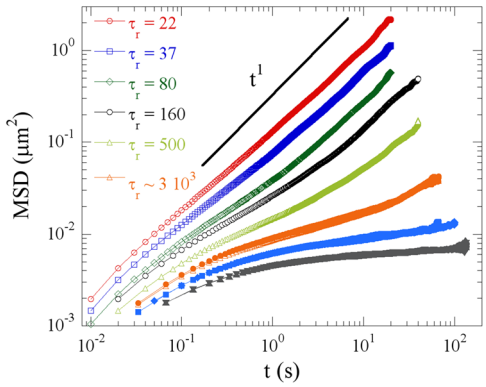

FIG. 10. Mean-squared displacement of latex tracers (0.994 μm in diameter) as a function of the lag time measured in the microgel suspensions. With increasing volume fraction, we observe a short-time diffusive behavior and then a sub-diffusive behavior at intermediate time scales. These two regimes are followed by a long-time diffusive behavior. At the highest volume fraction, a plateau develops and the crossover to the long-time diffusive regime could definitely not be reached within reasonable experimental timescales. A relative relaxation time τ_r is deduced from the long-time diffusion coefficient when measured.

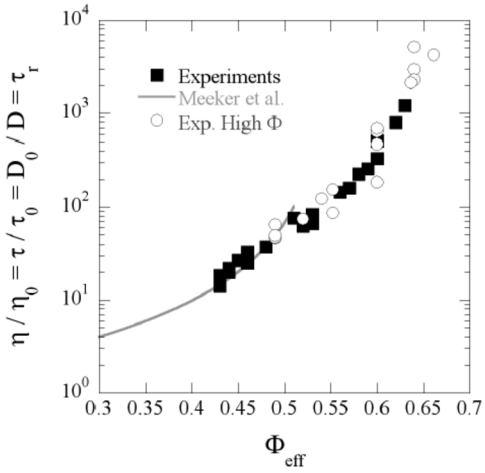

FIG. 11. Relative relaxation time as a function of an effective volume fraction in our microgel suspensions (○, ■). The straight line is obtained in hard spheres' suspensions, by Meeker *et al.*,[28] and provides a good description of our soft sphere suspensions up to $\Phi_{\text{eff}} = 0.5$. Around $\Phi_{\text{eff}} = 0.66$–0.70, the increase is sharp, giving an estimate of the glass transition volume fraction.

Figure 10 shows the MSD of latex tracers (0.994 μm in diameter) in the microgel suspension at various volume fractions. This latter parameter was increased in a quasistatic way, by performing temperature incremental step increases. The suspension was allowed to relax between each step to reach an equilibrium state.

From the mean-squared displacement data, one can infer a relative relaxation time τ_r and an effective volume fraction Φ_{eff}, whose calculation is already described in Sec. II. The relative relaxation time τ_r was deduced from the long-time diffusion coefficient D_∞, with $\tau_r = \tau(T)/\tau_0(T) = \eta(T)/\eta_0(T) = D_0/D_\infty$, where τ, η, and D_∞ and τ_0, η_0, and D_0 are, respectively, the probe diffusion time, viscosity, and long-time diffusion coefficient in the microgel suspension and in water. All the suspensions investigated, with varying the microgel density or volume fraction, follow a master curve—relative relaxation times versus effective volume fractions—shown in Fig. 11. It is similar to the master curve of Senff and Richtering[17] and gives evidence of the equivalence between both parameters. The relative relaxation time, or relative viscosity $\tau_r = \eta/\eta_0$, increases with volume fraction. For low volume fractions between $0.4 < \Phi_{\text{eff}} < 0.5$, the data obtained in hard sphere suspensions by Meeker *et al.*[28] provide a good description of our data. Around effective volume fraction $\Phi_{\text{eff}} = 0.66$–0.70, the increase is sharp, giving an estimate of the glass transition volume fraction.

Figure 10 shows that, at low volume fraction or relative relaxation time, the suspension is in a liquid state as characterized by the linear dependency of the MSD with the lag time. Upon increasing volume fraction, the MSD typically exhibits a short-time diffusive regime, followed by a sub-diffusive regime at intermediate time scales, and again a long-time diffusive regime, which can only be measured when the suspension is not too deep in the supercooled states. At the highest volume fractions (or reciprocally relative relaxation times), a plateau develops and the crossover to the long-time diffusive regime could definitely not be reached within reasonable experimental time scales.

We have previously shown that the signature of dynamical heterogeneities that characterize the supercooled regime was encapsulated in how the PDFs deviate from a Gaussian.[11,16] Based on their dynamical properties, our suspensions could be classified as follows. At low volume fraction, the MSD is linear and the PDF is Gaussian, revealing a liquid state. Upon increasing volume fraction, the PDF departs from a Gaussian, the MSD is non-linear, and the suspension equilibrates rapidly on the observation time scales (as demonstrated by the fast τ_r), which is the signature of a supercooled liquid. At large volume fractions, the PDF is highly non-Gaussian (exponential decay of the PDF over several decades[11]), the suspension equilibrates on large observation time scales as demonstrated by large τ_r around 3000, the MSD develops a plateau, and the long-time diffusive regime could definitely not be reached within reasonable experimental time scales, which will be classified as a glass.

The curves presented in this study, with relatively large relaxation times $\tau_{r29} = 128 \pm 7$ and $\tau_{r27} = 649 \pm 32$ and non-Gaussian PDFs, are in the supercooled state.

APPENDIX B: ACTIVITY FOR A BROWNIAN MOTION

Our Brownian particle has diffusion constant D. We ask how the activity of a given particle with trajectory $\mathbf{r}(t)$ is distributed. The generating function $\hat{P}(s,t) = \langle e^{-sK(t)} \rangle$ of the activity is written as $\hat{P}(s,t) = \langle e^{-s\sum_{m=0}^{M-1} \Theta(||\Delta \mathbf{r}_m - a)} \rangle$, where $\Delta \mathbf{r}_m = \mathbf{r}((m+1)\Delta t) - \mathbf{r}(m\Delta t)$. Using that all segments of the trajectory are independent, we end up with $\hat{P}(s,t) = \langle e^{-s\Theta(||\Delta \mathbf{r}||-a)} \rangle^M$. The argument in between the average brackets is unity if the excursion $||\Delta \mathbf{r}||$ remains smaller than a and e^{-s} otherwise. As defined, our activity is thus a positive number varying between 0 and M. Given that the probability of a displacement $\ell = ||\Delta \mathbf{r}||$ is, in 3d, $p(\ell, \Delta t) = \frac{4\pi \ell^2}{\sqrt{4\pi D \Delta t}^3} e^{-\frac{\ell^2}{4D\Delta t}}$, we arrive at

$$\hat{P}(s,t) = \left[\int_0^a d\ell p(\ell, \Delta t) + e^{-s} \int_a^\infty d\ell p(\ell, \Delta t) \right]^M . \quad \text{(B1)}$$

Once the generating function $\hat{P}(s,t)$ is known, one can reconstruct the full distribution by inverting the Laplace transform according to $P(K,t) = \int \frac{ds}{2\pi i} e^{sK} \hat{P}(s,t)$. At asymptotically large times, one can find the behavior of $P(K, t)$ to be given, in terms of $k = \frac{K}{M}$ and $u = \frac{a}{\sqrt{D\Delta t}}$, by

$$\frac{\ln P(K,t)}{M} \simeq k \ln \left[\frac{\operatorname{erfc}\left(\frac{u}{2}\right) - 1 + \frac{u e^{-\frac{u^2}{4}}}{\sqrt{\pi}}}{k-1} \right] + k \ln \left[\frac{k-1}{k} \frac{\frac{u e^{-\frac{u^2}{4}}}{\sqrt{\pi}} + \operatorname{erfc}\left(\frac{u}{2}\right)}{\frac{u e^{-\frac{u^2}{4}}}{\sqrt{\pi}} - \operatorname{erf}\left(\frac{u}{2}\right)} \right]. \tag{B2}$$

The average activity maximizes $P(K, t)$ and it reads

$$\frac{\langle K \rangle}{M} = \begin{cases} \operatorname{erfc}\left(\frac{u}{2}\right) + \frac{e^{-\frac{u^2}{4}} u}{\sqrt{\pi}} & (d=3), \\ e^{-\frac{u^2}{4}} & (d=2), \end{cases} \tag{B3}$$

and the right-hand side in (B3) is bounded by 0 and 1. Asymptotic expressions for the higher moments or the cumulants of K can be found by similar means. The variance is given by

$$\langle K^2 \rangle_c = \begin{cases} M(e^{-\frac{u^2}{4}} - e^{-\frac{u^2}{2}}) & \text{if } d=2, \\ \frac{M e^{-\frac{u^2}{2}} \left(\sqrt{\pi} e^{\frac{u^2}{4}} \operatorname{erf}\left(\frac{u}{2}\right) - u\right) \left(\sqrt{\pi} e^{\frac{u^2}{4}} \operatorname{erfc}\left(\frac{u}{2}\right) + u\right)}{\pi} & \text{if } d=3, \end{cases} \tag{B4}$$

and the first nontrivial signature of a deviation with respect to the Gaussian distribution, namely, the normalized third cumulant, otherwise known as the skewness κ_3 of the distribution reads

$$\kappa_3 = \frac{1}{\sqrt{M}} \frac{e^{-\frac{u^2}{4}} \left(\sqrt{\pi} e^{\frac{u^2}{4}} \left(2\operatorname{erf}\left(\frac{u}{2}\right) - 1\right) - 2u\right)}{\sqrt{\sqrt{\pi} e^{-\frac{u^2}{4}} u \left(2\operatorname{erf}\left(\frac{u}{2}\right) - 1\right) - \pi \left(\operatorname{erf}\left(\frac{u}{2}\right) - 1\right) \operatorname{erf}\left(\frac{u}{2}\right) - e^{-\frac{u^2}{2}} u^2}}. \tag{B5}$$

A similar calculation carried out in space dimension 2 leads to

$$\frac{\ln P(K,t)}{M} \simeq -\frac{ku^2}{4} + \ln\left(\frac{e^{-\frac{u^2}{4}} - 1}{k-1}\right) + k \ln\left(-\frac{(k-1)\left(\coth\left(\frac{u^2}{8}\right) + 1\right)}{2k}\right) \tag{B6}$$

along with

$$\kappa_3 = \frac{1}{\sqrt{M}} \frac{-2 + e^{\frac{u^2}{4}}}{\sqrt{-1 + e^{\frac{u^2}{4}}}}. \tag{B7}$$

APPENDIX C: RESULTS FROM WEEKS DATA ANALYSIS

1. Description of the experimental system

A number of measurements have been performed to quantify the motion of colloidal particles near the glass transition. We focus here on the simplest system, i.e., monodisperse colloids (poly-methylmethacrylate particles stabilized by a thin layer of poly-12-hydroxystearic acid), both in equilibrated supercooled colloids fluids and non-equilibrated glasses, as used in the pioneering work on dynamical heterogeneities by Weeks *et al.*[27] The particles have a radius $a_0 = 1.18$ μm. We chose to analyze the 3d motion of particles recorded by confocal microscopy in two distinct systems. The first one is a supercooled fluid, with density $\phi = 0.46$, the time step between consecutive images is $\delta t_{0.46} = 10$ s, the duration of the movie is $271\delta t_{0.46}$, and the number of tracked particles is 4232. The second one is a glass studied after a long period of aging, with density $\phi = 0.6$, the time step between consecutive images is $\delta t_{0.6} = 120$ s, the duration of the movie is $333\delta t_{0.6}$, and the number of tracked particles is 5922. We have also analyzed the data concerning an intermediate system with density $\phi = 0.52$, which is a denser but still supercooled fluid, with time step between consecutive images being $\delta t_{0.52} = 18$ s, duration of the movie $431\delta t_{0.52}$ and the number of tracked particles is 4679. We will also present some of the results from this data set. We note that although most glassy samples are aging, this can be neglected over the duration of the measurements. The tracking procedure is hence different from ours: here the coordinates of all particles were tracked, whereas in our experiments, the motion of a few tracers only was recorded. Moreover, the time duration of the movies recorded in the work of Weeks *et al.*[27] is relatively short considering the displacements distribution function (the displacement do not exceed the particle radius a_0), whereas in our experiments, the movies are longer in the sense that the PDF of the displacements samples distances as far as ~6 times the particle radii $\sigma/2$ (this is compensated by higher tracer statistics). We computed the activity for different values of a and $\Delta t = t_{obs}/M$. In the following, Δt is expressed in units of δt. Systems and tracking approaches differ, and they will nevertheless be shown to point in the same direction.

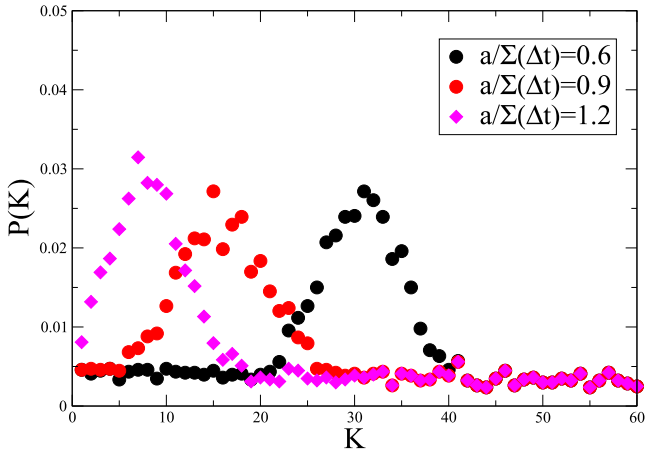

FIG. 12. Histogram of the activity K at $\phi = 0.46$ normalized by its average, $\Delta t = 6\delta t_{0.46}$, for three values of u equal to 0.6, 0.9, and 1.2. The histograms are symmetric.

2. Histogram of activity

In Figs. 12 and 13, we represent the distribution of activity for the three particle densities. The values of M that we have used range, for $\phi = 0.46$, from 20 to 40, for $\phi = 0.52$, from 50 to 100, and for $\phi = 0.6$, from 30 to 60. The denser (and more heterogeneous) system displays the strongest asymmetry when varying $a/\Sigma(\Delta t)$. In Fig. 14, we illustrate that the average of K does not allow us to distinguish dynamically and non-dynamically heterogeneous situations, in the same way as for our experimental data (see Fig. 3). The observed value for the average activity is very close to the analytical result (2) for Brownian particles in three dimensions.

3. Average variance of the activity

In Figs. 15 and 16, we illustrate (as for our experimental data in Figs. 6 and 7) that more glassy (denser) system displays an increase in the variance. The Brownian result (B4) (in dimension $d = 3$) serves as a comparison and is much smaller in all cases.

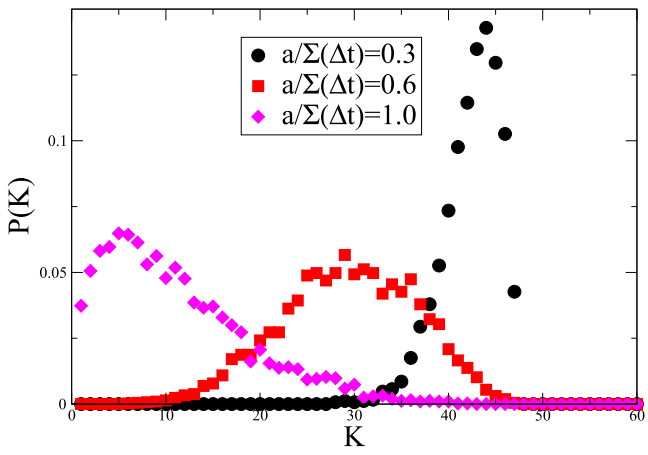

FIG. 13. Histogram of K at $\phi = 0.6$ normalized by its average, $\Delta t = 7\delta t_{0.6}$ for three values of u equal to 0.3, 0.6, and 1. The scaled skewness represented on 17 provides one a quantitative indicator that the sample at $\phi = 0.6$ is clearly heterogeneous, compared to the sample at $\phi = 0.46$, because of its clear departure from the purely Brownian behavior.

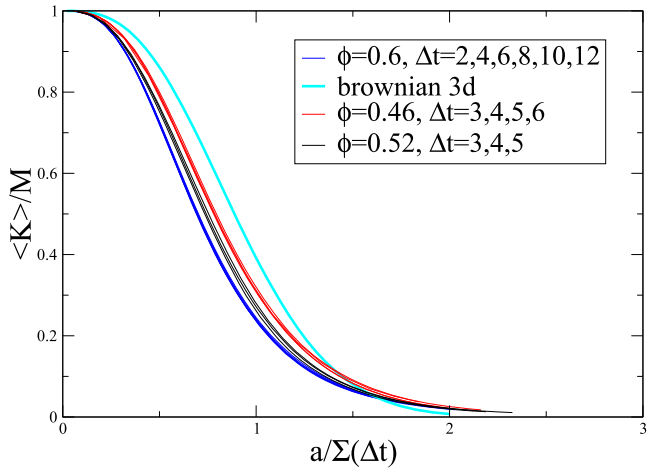

FIG. 14. Mean activity $\langle K\rangle/M$ at $\phi = 0.46$, 0.52, and 0.6 versus the Brownian result (2) (for $d = 3$ dimensions). For each density ϕ, Δts are expressed in units of δt_ϕ. The mean activity decreases only slightly as a function of density.

4. Scaled skewness of the activity

In Fig. 17, we illustrate (as for our experimental data in Figs. 8 and 9) that the more glassy (denser) system displays a strongly asymmetric skewness compared to the Brownian case. For $\phi = 0.46$, the skewness is very close to the Brownian case and close to zero for a large range of values of u, which is consistent with the symmetric histograms plotted in Fig. 12. For $\phi = 0.6$, the skewness is also the same as the Brownian case for small values of u but departs strongly from this behavior for u larger than 0.6. This is again consistent with the symmetries revealed in Fig. 13. In the same way we did for our experiment on pNIPAm, we interpret the excess of larger than average activity for large u as the manifestation of long range collective rearrangements (cooperatively rearranging regions) in glassier systems. However we observe that the skewness for small u is the same as in the Brownian case, hence one cannot see in these data an excess of less than average active events at small scales. This may be due to the differences in scales probed by the two experimental setups. In Weeks's experiments, small u corresponds to rattling inside a cage at very small length scales, whereas large u corresponds to escapes from the cages.

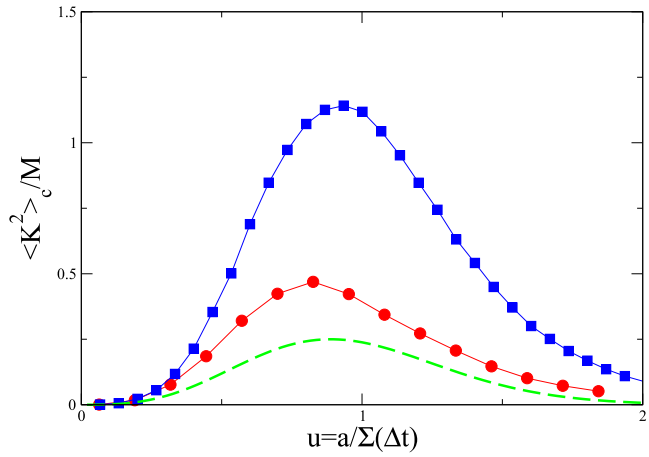

FIG. 15. Mean variance $\langle K^2\rangle_c/M$ as a function of u at $\phi = 0.46$ and 0.52 for the same $\Delta t = 9\delta t_{0.46} = 5\delta t_{0.52} = 90$ s.

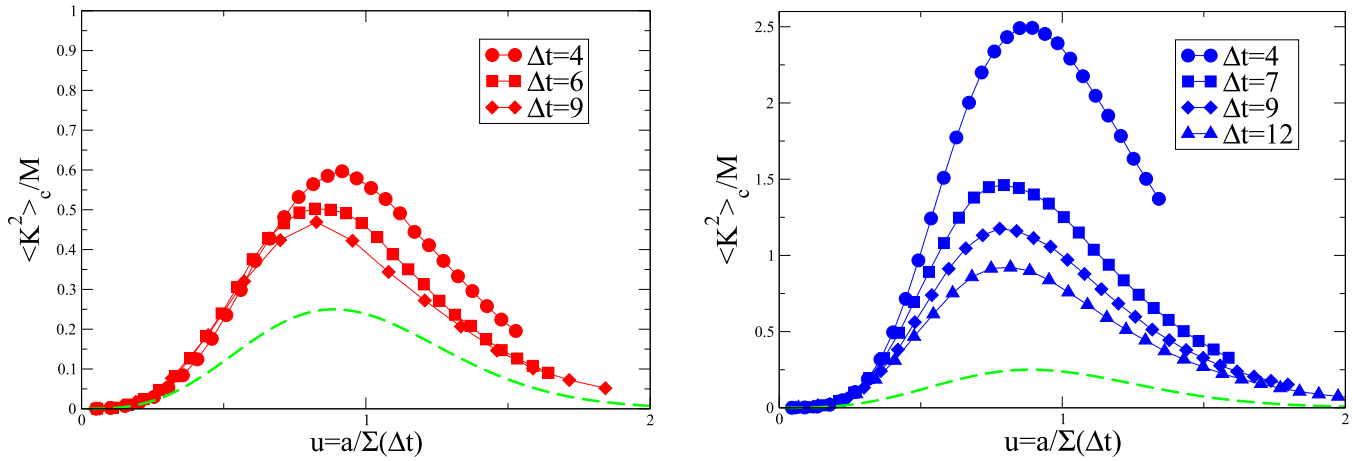

FIG. 16. Mean variance $\langle K^2\rangle_c/M$ as a function of u for the 2 densities $\phi = 0.46$ and $\phi = 0.6$ and different values of Δt expressed as units of δt_ϕ. The Brownian curve is plotted as a reference.

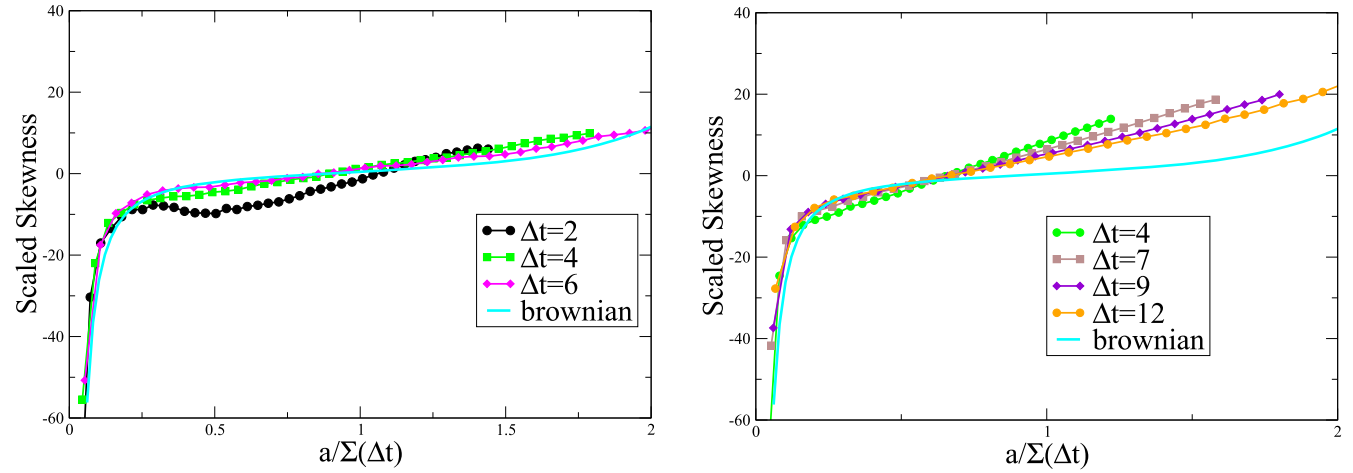

FIG. 17. (Right) Scaled skewness $\kappa_3\sqrt{M}$ at $\phi = 0.6$ for varying values of Δt in units of $\delta t_{0.46}$. (Left) Scaled skewness $\kappa_3\sqrt{M}$ at $\phi = 0.46$ for varying values of Δt in units of $\delta t_{0.6}$.

In our experiments, the same difference in scales is true but a single movie will probe more escapes from cages, and less rattling motions, than in Weeks' setup. We believe that if the time scale of Weeks' experiments was comparable to ours, the departure from Brownian at negative skewness would also be visible.

[1] F. Ritort and P. Sollich, Adv. Phys. **52**, 219 (2003).
[2] L. Berthier, *Dynamical Heterogeneities in Glasses Colloids and Granular Media*, International Series of Monographs on Physics (Oxford University Press, Oxford, 2011).
[3] T. R. Kirkpatrick, D. Thirumalai, and P. G. Wolynes, Phys. Rev. A **40**, 1045 (1989).
[4] S. Gokhale, K. Hima Nagamanasa, R. Ganapathy, and A. K. Sood, Nat. Commun. **5**, 4685 (2014).
[5] S. Gokhale, R. Ganapathy, K. H. Nagamanasa, and A. K. Sood, Phys. Rev. Lett. **116**, 068305 (2016).
[6] J. Garrahan, R. Jack, V. Lecomte, E. Pitard, K. van Duijvendijk, and F. van Wijland, Phys. Rev. Lett. **98**, 195702 (2007).
[7] L. O. Hedges, R. L. Jack, J. P. Garrahan, and D. Chandler, Science **323**, 1309 (2009).
[8] E. Pitard, V. Lecomte, and F. van Wijland, Europhys. Lett. **96**, 56002 (2011).
[9] D. Ruelle, *Thermodynamic Formalism: The Mathematical Structure of Equilibrium Statistical Mechanics*, Cambridge Mathematical Library (Cambridge University Press, 2004).
[10] R. Pinchaipat, M. Campo, F. Turci, J. E. Hallett, T. Speck, and C. P. Royall, Phys. Rev. Lett. **119**, 028004 (2017).
[11] R. Colin, A. M. Alsayed, J.-C. Castaing, R. Goyal, L. Hough, and B. Abou, Soft Matter **7**, 4504 (2011).
[12] A. S. Keys, L. O. Hedges, J. P. Garrahan, S. C. Glotzer, and D. Chandler, Phys. Rev. X **1**, 021013 (2011).
[13] T. Speck and D. Chandler, J. Chem. Phys. **136**, 184509 (2012).
[14] A. S. Keys, J. P. Garrahan, and D. Chandler, Proc. Natl. Acad. Sci. U. S. A. **110**, 4482 (2013).
[15] R. Colin, A. M. Alsayed, C. Gay, and B. Abou, Soft Matter **11**, 9020 (2015).
[16] R. Colin, "Suspensions de microgels thermosensibles à la transition vitreuse: Dynamique hétérogène, corrélation, fluctuation et réponse rotationelles d'aiguilles," Ph.D. thesis, Université Paris-Diderot–Paris VII, 2012, https://tel.archives-ouvertes.fr/tel-00751204v1.
[17] H. Senff and W. Richtering, J. Chem. Phys. **111**, 1705 (1999).
[18] J. Mattsson, H. M. Wyss, A. Fernandez-Nieves, K. Miyazaki, Z. Hu, D. R. Reichman, and D. A. Weitz, Nature **462**, 83 (2009).
[19] C. Crauste-Thibierge, C. Brun, F. Ladieu, D. L'Hôte, G. Biroli, and J.-P. Bouchaud, Phys. Rev. Lett. **104**, 165703 (2010).
[20] Note that in a simple fluid phase, a single peak is observed.
[21] V. Chikkadi, D. Miedema, M. Dang, B. Nienhuis, and P. Schall, Phys. Rev. Lett. **113**, 208301 (2014).
[22] V. Lecomte, C. Appert-Rolland, and F. van Wijland, Phys. Rev. Lett. **95**, 010601 (2005).
[23] V. Lecomte, C. Appert-Rolland, and F. van Wijland, J. Stat. Phys. **127**, 51 (2007).